ICES Journal of Marine Science, 60: 1232–1250. 2003
doi:10.1016/S1054–3139(03)00137-1

Spring–summer climatological circulation in the upper layer in the region of Cape St. Vincent, Southwest Portugal

Ricardo F. Sánchez and Paulo Relvas

Sanchez, R. F., and Relvas, P. 2003. Spring–summer climatological circulation in the upper layer in the region of Cape St. Vincent, Southwest Portugal. – ICES Journal of Marine Science, 60: 1232–1250.

Geostrophic transport and hydrographic measurements derived from a historical database (1900–1998) were used to study the spring–summer mean circulation in the upper layer south and west of Cape St. Vincent, Southwest (SW) Portugal. The larger-scale circulation scheme is forced by equatorward winds from May to September, when the Iberian coastal transition zone (CTZ) is dominated by a generalized upwelling of cold, low-salinity water. A partially separated surface jet intensified at the shelf break conveys ~1 Sv of upwelled water equatorward parallel to the bathymetry, while offshore a poleward flow transports ~0.4–0.6 Sv of upwelled water. Although alongshore transports dominate the circulation pattern of the upper layers, cross-shore transports are significant at the climatological scale. Anticyclonic circulation with an exchange of ~0.5 Sv from the equatorward jet to the offshore poleward flow and the partial re-circulation further north, back into the equatorward flow are discussed. A coherent, cyclonic re-circulation pattern inshore of the upwelling jet is also speculated. From these results the shelf break is considered a climatological border at both sides of which two major re-circulation cells occur. The climatological equatorward flow has offshore protrusions, interpreted as recurrent episodes of major contortions of the upwelling flow. These features bring about considerable "cross-shelf flow" re-circulation reaching up to 50% of the main flow. The most significant exchanges are found to be associated with major changes of orientation of the coastline. Off Cape St. Vincent the upwelling front stretches to both west and south and contributes to the cross-shelf re-circulations. Additionally, convergence of the upwelling flow and a branch of the Azores current, with associated re-circulation is found diagonally from the cape. On the southern coast the upwelling jet is seen to meander offshore in the vicinity of Cape St. Maria. Individual synoptic cruise data showed agreement with the climatological circulation features. We conclude that these oceanographic features leave an imprint on the climatic circulation in spite of the "smoothing out" of recurrent events over the spring–summer period of the years of 1900–1998.

Keywords: coastal transition zone, re-circulation, summer upwelling, transport, upwelling filaments, water exchange.

Received 9 October 2002; accepted 10 February 2003.

R. F. Sánchez: CIACOMAR – Universidade do Algarve, Av. 16 Junho s/n, 8700-311 Olhão, Portugal. P. Relvas: CIMA – Universidade do Algarve (FCMA), Campus de Gambelas, P-8000-117 Faro, Portugal; e-mail: prelvas@ualg.pt. Correspondence to R. F. Sánchez; tel: +351 289707087; fax: +351 289706972; e-mail: rleal@ualg.pt.

Introduction

The eastern boundaries of the oceans are recognized as complex current systems (Brink *et al.*, 2000). The eastern boundary current (EBC) system off the coast of the Iberian Peninsula (IP) has been acknowledged as a seasonally dependent, two-layered current system with similarities to the California current system (CCS) (Haynes *et al.*, 1993). These regions, together with the area off the northwest African coast, are among the most studied "coastal transition zones" (CTZs) of the world oceans.

Off the Atlantic coast of the IP the Portugal current has been treated as a portion of the Canary current (CC), an upper-layer, equatorward flow that lies off the Iberian west coast (e.g. Tomczak and Godfrey, 1994) influenced by upwelling-favourable winds. Along the continental slope (~300–500 m) the flow is markedly poleward (Fiúza, 1982), and a two-layered current system may be set up. This undercurrent, also known as the Iberian poleward current (IPC), appears as a narrow (~25–40 km), relatively weak (less than ~20 cm s^{-1}) slope-intensified flow that advects subtropical water northwards (Haynes and Barton,

1990). In winter this flow reaches the surface and can be traced with Advanced Very High Resolution Radiometer (AVHRR) satellite imagery. It has been tracked to extend into locations as far north as the Goban Spur (north of 48°N) (Pingree, 1993).

The apparent contradiction between the classical notion of a southward Portugal current (Krauss and Käse, 1987; Arhan *et al.*, 1994) and the net poleward flow described by some authors (Haynes and Barton, 1990; Mazé *et al.*, 1997) has been solved via consideration of the seasonality of the Iberian eastern boundary. The Azores High (AH) experiences seasonal, meridional displacements, and the associated large-scale wind patterns cause distinct winter and summer oceanographic regimes off the IP CTZ. Winter southward migration of the AH causes a mean E–W pressure contrast between Portugal and the centre of the AH of ∼1 mb resulting in weak and variable winds. Conversely, the summer reinforcement of circulation brings about a ∼8 mb pressure contrast and strong northerly to northwesterly (upwelling-favourable) winds (Chase, 1956), which force an offshore Ekman transport in the upper ocean, leading to a generalized upwelling of cold and nutrient-rich water from below the pycnocline. As an oceanic geostrophic response to the prevailing winds, a cool, equatorward surface jet flows over the shelf break along the west coast over the 100–300 m isobath. The upwelling conditions that are seasonal along the west coast take place only occasionally along the southern coast, when upwelling-favourable westerly winds blow locally and the flow proceeds eastward along the southern coast. However, even during north-wind cycles upwelled waters may be conveyed along the southern shelf break by an eastward extension of the upwelling jet (Fiúza, 1983).

The summer circulation pattern in the CTZ is much more complicated than a simple band of cold, upwelled water. Shorter-term fluctuations are superimposed on the more stable variations at seasonal timescales and a host of mesoscale structures such as jets, meanders, ubiquitous eddies, squirts and upwelling filaments have been observed (e.g. Haynes *et al.*, 1993; Huthnance, 1995; Smith, 1995). Such filaments are not simply superficial structures and, indeed, they have clear biological and chemical signatures. The cold surface waters tend to be enriched in nutrients and are typically accompanied by rather high concentrations of phytoplankton biomass (e.g. Traganza *et al.*, 1980) as well as other biological material such as fish larvae associated with the neritic domain (e.g. Rodríguez *et al.*, 1999).

In this paper the spring–summer hydrographic structure of the upper layer west and south of Cape St. Vincent, Southwest (SW) Portugal (Figure 1), is defined from the analysis of historical data. Then, the mean geostrophic transport is presented with the aid of the dynamic topography and geostrophic velocity structure. Next, a climatic view of the circulation scheme in the upper layer is outlined. Finally, relevant features of the spring–summer circulation regime are validated with *in situ* data.

Methods

The present study is based on ∼16 000 individual hydrographic stations located along the southwestern Portuguese coast between 1900 and 1998 in the region bounded by 10°30′W–6°W and 35°42′N–40°N (Figure 1a and b). The data were obtained from several sources: 80% from the World Ocean Database 1998, version 2.0, January 2000, prepared by the Ocean Climate Laboratory of the National Oceanographic Data Centre (NODC, 2000) and the remaining 20% from the British Oceanographic Data Centre (BODC), the Systèmes d'Informations Scientifiques pour la Mer (SISMER – IFREMER) and a local database.

To evaluate mean spring–summer conditions, only profiles acquired between May and September were included. Data were quality-controlled to eliminate erroneous

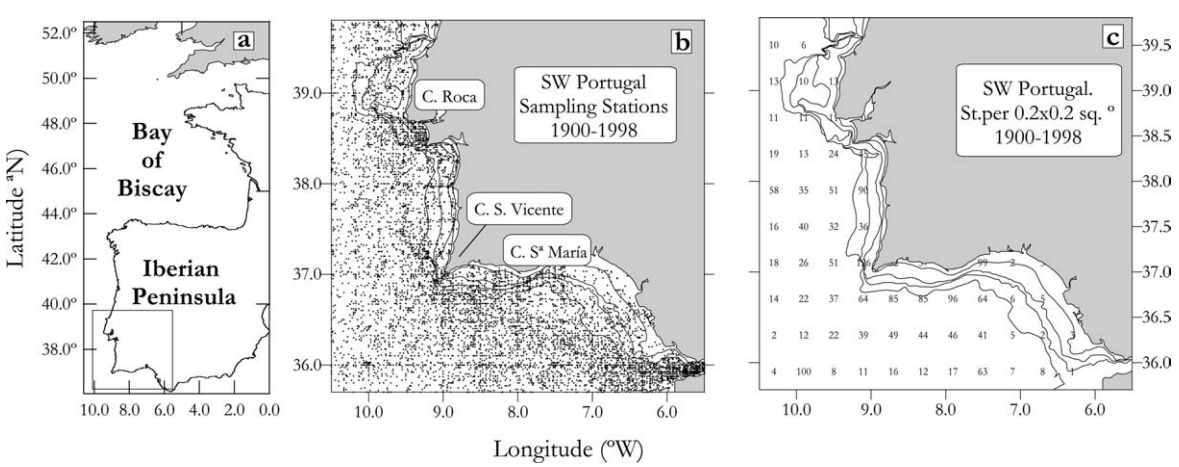

Figure 1. (a) The area of the study. (b) The set of observations off SW Portugal. (c) The number of valid profiles per 0.2° × 0.2° square, and the 30, 100, 200 and 400 m bathymetric contours.

or badly referenced data. Data-processing protocol followed Lozier *et al.* (1995) who also worked with the NODC database. Whilst similar quality-control steps are used here, modifications had to be done given the finer resolution and the reduced size of our data set. All data were pre-processed with the Ocean Data View software (Schlitzer, 2001), which proved to be a very helpful tool for the visualization and pre-analysis of the climatological data set. First, a range check as a function of depth was applied and values outside broad property ranges were eliminated. The temperature–salinity (T–S) curve was approximated by subdividing the observed points into density bins for which the mean T–S relation was approximately linear. The standard deviation of the observations was computed for each bin. T–S scatter plots for all stations were constructed. These plots graphically showed data points that deviated significantly from the mean line. Only points that lay within $\pm$ 2–3 standard deviations of the mean were retained as acceptable observations. This limit was chosen on the statistical basis that ~98% of all observations in a normally distributed population fall within 2–3 standard deviations on either side of the mean (e.g. Lozier *et al.*, 1995). Handpicking of outliers operated as a statistical check. A computational selection based on the same principles was run after the selection by hand. The quality check resulted in ~2000 quality-controlled, spring–summer profiles. Their distribution per $0.2^\circ \times 0.2^\circ$ square cells is presented in Figure 1c. From these profiles, quasi-synoptic subsets corresponding to single cruises that provided snapshots of the circulation were retrieved.

For each station the data were linearly interpolated every 10 m in the vertical to project a property value onto a set of pressure surfaces. As sampling stations were sparsely distributed both in time and space, data were objectively analysed with a simple, isotropic, univariate interpolation method. An objective technique with scale separation developed by Doswell (1977) and Maddox (1980), based on the filtering properties of the objective analysis scheme developed by Barnes (1964), was applied. It stems from the values of neighbouring data and on an assumed correlation function of the field. The correlation scale was set to 20 km as used by Ochoa and Bray (1991), while the number of interpolations was set at 70 to permit error variances of O(1) for temperature, O(0.1) for salinity and density anomaly and O(0.01) for dynamic height, which accounted for the previous smoothing of the observations. Additionally, the analysis operated as a low-pass filter, filtering the observed data field to define the analysed field. The band-pass response of the filtering was centred at a wavelength of 70 km. The short-wavelength noise was therefore filtered out. The result was a matrix of gridded, smoothed values interpolated at 12′ longitude by 8.4′ latitude (18×16 km^2) cells and vertically interpolated every 10 m.

The geostrophic transport was calculated on the 400-m reference level according to the following algorithm (UNESCO, 1991):

$$T = L \int_{Z_n}^{Z_o} (v - v_r)\, dz$$

where $v - v_r$ is the geostrophic velocity (v) relative to the reference level (v_r), L is the distance between two grid points and Z_o and Z_n are the vertical limits of integration. The selection criterion of the reference level of dynamic topography was based on the compromise between the spatial distribution of sampling points and the need to avoid the Mediterranean Outflow (MOW). Ambar (1983) indicated the existence of a shallow MOW core at ~400 m in the Gulf of Cadiz. Additionally, a seasonal analysis permitted the observation that the spring–summer dynamics of the eastern North Atlantic Central Waters (eNACW) along the study region could be characterized by the upper 400 m layer (see Results). Hence the 400-m level proved to be the most suitable choice for the reference level of dynamic topography. To provide reasonable coverage along the inshore region nearly 200 shelf stations retrieved from the synoptic subsets that did not reach 400 m were extrapolated to the bottom following the extrapolation method proposed by Reid and Mantyla (1976).

Monthly means of sea surface temperature (SST) and sea surface wind (SSW) were obtained from the Comprehensive Ocean–Atmosphere Data Set (COADS). Wind stress ($\boldsymbol{\tau}$, N m^{-2}) was calculated as (bold types indicate vector units)

$$\boldsymbol{\tau} = \rho_a * C_d * \mathbf{u} * |\mathbf{u}| \quad (1)$$

where ρ_a is air density (a value of 1.22 kg m^{-3} was assumed), $\mathbf{u}$ is surface wind velocity in m s^{-1} and C_d is a non-linear drag coefficient (based on Large and Pond (1981) modified for low wind speeds as in Trenberth *et al.* (1990))

$$C_d = 0.00218 \text{ for } |\mathbf{u}| \leq 1 \text{ m s}^{-1}$$

$$C_d = (0.62 + 1.56 * |\mathbf{u}| - 1) * 0.001 \text{ for } 1 < |\mathbf{u}| < 3 \text{ m s}^{-1}$$

$$C_d = 0.00114 \text{ for } 3 \text{ m s}^{-1} \leq |\mathbf{u}| < 10 \text{ m s}^{-1}$$

$$C_d = (0.49 + 0.065 * |\mathbf{u}|) * 0.001 \text{ for } |\mathbf{u}| \geq 10 \text{ m s}^{-1}$$

Ekman transport (kg s^{-1} m^{-1}) has been calculated from the monthly wind stresses using the Ekman relation

$$\mathbf{E_k} = \boldsymbol{\tau} * f - 1 \quad (2)$$

where f is the Coriolis parameter. Ekman pumping results from Ekman-flux divergence and convergence, which in turn are caused by a spatially variable wind field. In order to conserve mass, a vertical velocity $\mathbf{w}$ results, which is (Gill, 1982)

$$\mathbf{w} = \mathbf{k}[\mathbf{curl} \times (\boldsymbol{\tau} * (\rho_o * f) - 1] \quad (3)$$

where $\times$ represents vector product, ρ_o is the density of seawater and $\mathbf{k}$ is the vertical unit vector.

Results

The annual cycle of SST, wind vectors and Ekman transport for the latitude 37°30′N (Figure 2) shows that the IP coast at 37°30′N is affected by northerlies throughout the year. It is during the months of April–September that the wind and associated Ekman transport are strongest, the maximum occurring in July (>600 kg m^{-1} s^{-1}) (Figure 2a). From November to March the southward drift of the AH affects the wind regime and consequently the wind stress is reduced and the Ekman transport falls to an annual minimum in January (<50 kg m^{-1} s^{-1}). The peak of summer heating occurs from July to October when SST exceeds 19.5°C (Figure 2b). While the isotherms remain zonal in winter, the maximum temperature contrast between the coast and the offshore region occurs between June and October, accompanying the seasonal cadence of the wind cycle. It is thus possible to define an upwelling season as a response to the strongest wind-forcing in summer at about the same time as the strongest heating. Fiúza *et al.* (1982) showed that the mean N wind stress and SST anomalies between the coast and 30°W show lagged correlation coefficients >0.9, with a lag of 1 month. Therefore Portuguese coastal upwelling occurs from July to September as a consequence of the intensity and persistence of northerly winds from June to August (Fiúza *et al.*, 1982).

The mean fields of SSW and Ekman transport, wind-stress curl and resulting vertical velocity at the base of the Ekman layer were calculated for the periods May–September and November–February at 1° interval by a centred-difference scheme from the COADS data (1960–1997). Figure 3a and c show the major geographic and seasonal variations of SSW and Ekman transport. During the summer months (Figure 3a) the wind vigorously blows from the north along the IP and African coast. Maximum wind velocities and consequent Ekman transports occupy a fringe parallel to the coast from 30°N to 43°N with intensity increasing southward and with maxima along the African coast. In winter there is a weakening of the climatological, equatorward winds south of 43°N, as a response to the southward migration of the AH (Figure 3d). This situation corresponds with generalized strengthening of westerlies north of 43°N.

Upwelling along the Portuguese region is strongly season-dependent, unlike off the African coast where the seasonal cycle is much weaker and the Ekman layer is divergent throughout the year (Figure 3b and e). The mean wind-stress-curl distribution is weak and irregular during fall and early winter, but becomes cyclonic during spring and summer, when spatially separated wind-stress-curl maxima appear adjacent to the northwestern coast of the IP and off southern Portugal. From May to September the Ekman layer is divergent from the coast out to 11–12°W, i.e. within 100–150 km of the IP coast during the summer coastal-upwelling maxima. Local positive maximum curl values are associated with major topographic changes in the coastline geometry such as around capes as already noted by Bakun and Nelson (1991). Maximum pumping velocities are of O(0.2) m day^{-1}, although this value is believed to be an underestimate (Saunders, 1976). Climatological

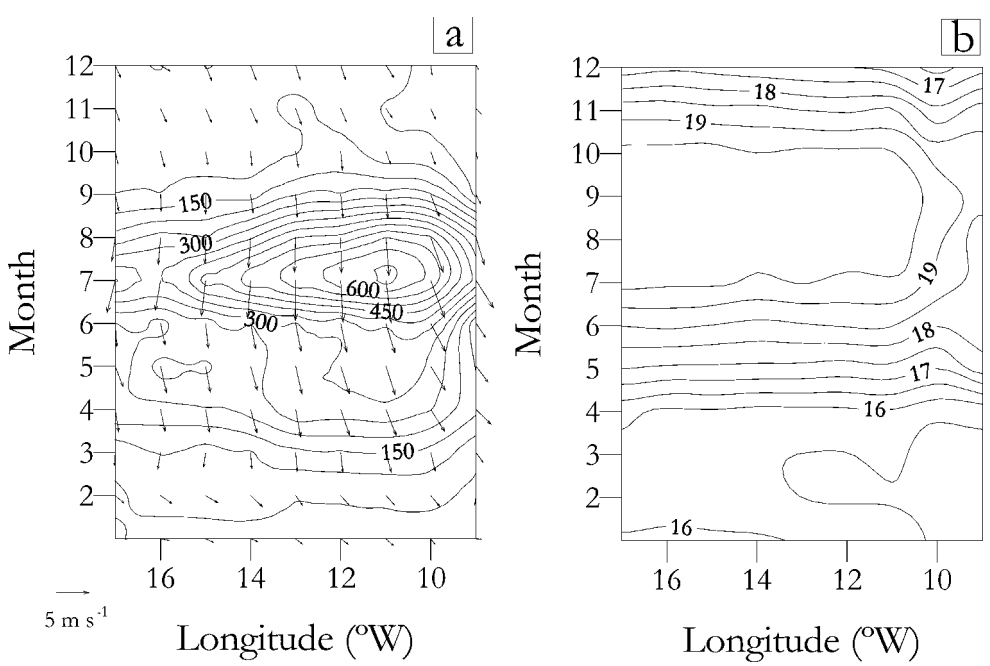

Figure 2. (a) The annual cycle at 37°30′N of monthly wind vectors (m s^{-1}) and contours of Ekman transport (kg m^{-1} s^{-1}). The wind reference vector is also shown. (b) The annual cycle of monthly SST (°C) at 37°30′N (source: COADS 1960–1997 data).

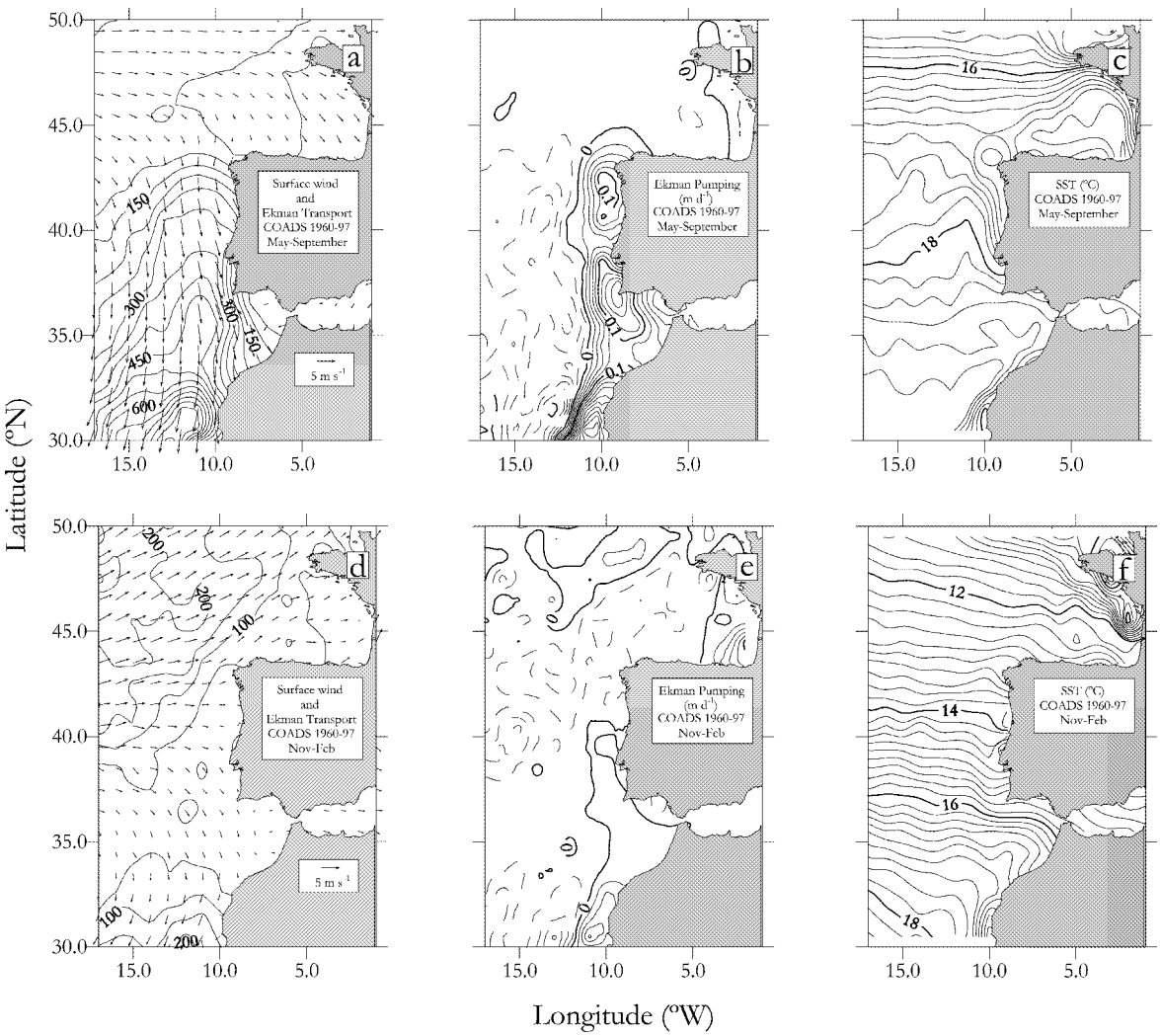

Figure 3. (a) Surface wind vectors (m s^{-1}) and contours of Ekman transport (kg m^{-1} s^{-1}) with the wind reference vectors shown, (b) the vertical velocity at the base of the Ekman layer (m day^{-1}) and (c) mean SST for May–September (°C). (d), (e) and (f) are the same as (a), (b) and (c) but for November–February (source: COADS 1960–1997 data).

estimates of wind stress are much lower than synoptic measurements (see Nelson (1977) and Enríquez and Friehe (1995) for the coast of California), and resulting Ekman pumping estimates may be smoothed by a factor of up to 40 over certain areas. This discrepancy is attributed to the reduction of the horizontal variability of the wind stress by using the averaged ship-report data set.

The climatic SST picture (Figure 3c and f) shows that the eastern boundary of the North Atlantic adjacent to the IP features a zonal distribution of isotherms off the continental shelf in summer. Southward deflection of isotherms over the shelf region breaks the zonal distribution (Figure 3c) and nearshore cooling is revealed even in the 1° grid resolution of this data set. Several studies point out the relationship of coast–mid-ocean temperature differences and the Ekman transport normal to the coast (or upwelling index) (Fiúza *et al.*, 1982; Nykjaer and Van Camp, 1994). Ekman transport peaks during the summer months (e.g. Figure 3a and d). Seasonal development of a band of cold water fringing the coast results as a consequence of spring–summer upwelling winds off the IP. More permanent coastal upwelling and a smoother SST cycle are found off the West African coast.

The monthly mean annual cycle of water column temperature and salinity around the Cape St. Vincent computed from the NODC archive for the box 38°30′–35°30′N, 10°–8°W (Figure 4) shows intensified thermal stratification at the surface from May, just at the start of the strongest northerlies, till the end of November, after the climatological winds have fallen to the winter minimum (e.g. Bakun and Nelson, 1995) (Figure 4a). During this period the upper 100 m shows the maximum temperatures

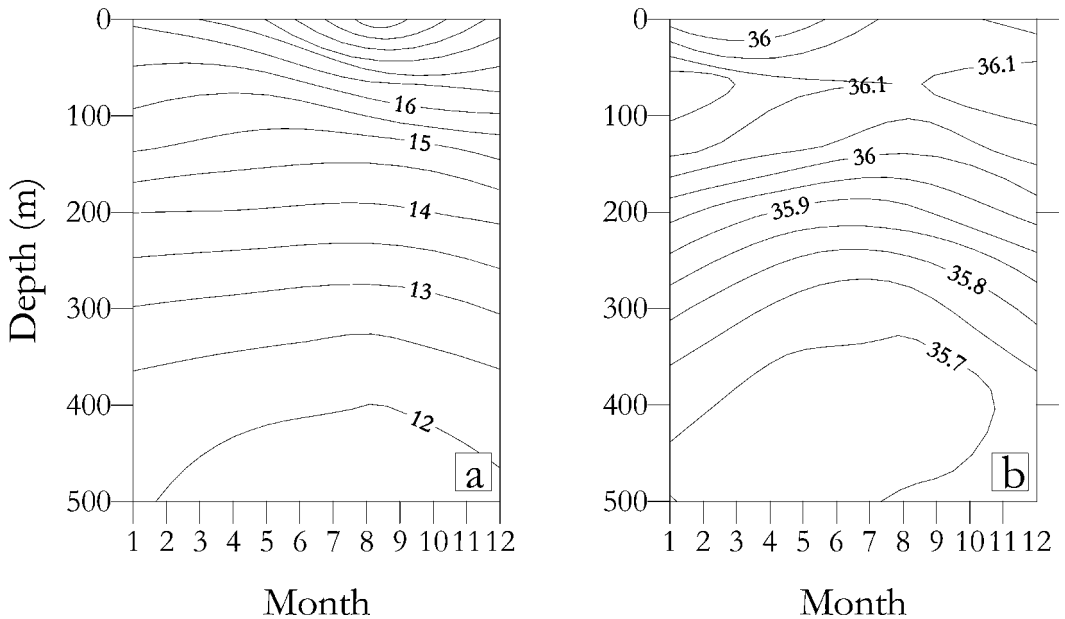

Figure 4. (a) The mean annual cycle of water column temperature (°C) and (b) the salinity for the box 38°30′–35°30′N, 10°–8°W around the Cape St. Vincent (source: monthly averages from the NODC archive).

due to solar warming plus stirring by strong winds: note the 16°C line. Upper-ocean temperature variations show a time lag with respect to the atmospheric variations (−1 month, as observed by Fiúza *et al.* (1982)) and the oceanic summer extends well into the meteorological autumn. Below 400 m there is also a seasonal cycle opposing that of surface waters (cf. 12°C line).

There is a salinity maximum at ∼100 m that outlines the extent of the surface mixed layer. Below, salinity values decrease with depth down to the salinity minimum that marks the deepest extent of eNACW over the MOW (Figure 4b). Seasonality also affects the salinity structure, and the annual cycle of salinity shows a sinusoidal trend. At the surface maximum values are centred from June to October. This feature may be interpreted as the response of the upper stratum of the water column to the seasonal salinity cycle in middle latitudes, possibly strengthened by the wind-induced, spring–summer coastal upwelling. The subsurface salinity minimum (<35.7) rises up to 400 m in summertime and descends to 475 m in December. The uplift of this salinity minimum together with the seasonal cycle of mid-depth water temperatures could be related to the seasonal cycle of the MOW that is observed to be at its maximum in the spring–summertime (Bormans *et al.*, 1986; Ochoa and Bray, 1991). The possibility remains that this cycle could be strengthened by the wind-induced, spring–summer coastal upwelling.

Hydrographic structure from the historical data

T–S curves of all stations in the analysis are depicted in Figure 5a. The high salinities of the MOW for densities >27.2 are evident. Above, the T–S curves exhibit a salinity minimum at ∼450 m. Both temperature and salinity increase upwards to the bottom of the seasonal thermocline, where a slight salinity maximum can be observed for most stations at ∼100 m (Figure 4b). These waters adjust to the tight relationship defined for eNACW of subtropical origin (e.g. Fiúza and Halpern, 1982). However, while the mean salinities of thermocline waters in summer are in the range ∼36–36.1 (Figure 4b), there is a great deal of variability, as observed in Figure 5a. This variability is attributable to the seasonal coastal upwelling and to the input of the climatological Azores current (AC).

As a result of the upwelling-favourable winds, from May to September most of the nearshore area is occupied by cold and low-salinity waters whose source is the coastal upwelling (Figure 6a and b). At the upper layers (10 m) these waters are characterized by T values between 14 and 18.5°C and S values below 36.16. This general pattern was interrupted east of 7°30′W, where coastal upwelling is not such a recurrent spring–summer feature (Fiúza, 1983). In the easternmost Gulf of Cadiz a well-defined pool of warm waters is seen to prevail. Upwelled waters are separated from the warmer (>19°C) and more saline (>36.2) waters offshore by an intense front. Thermal and haline gradients are intensified off the most prominent capes, such as Cape Roca (3.5°C per 50 km and 0.4 per 50 km), where the strongest density gradients are also observed (1 kg m^{-3} per 50 km; not shown). The upwelling front runs parallel to the coastline geometry. There is also another thermohaline front that separates surface waters north and south of ∼37°N. This front can be associated with the climatological Azores current, as Lozier *et al.* (1995) have already pointed out.

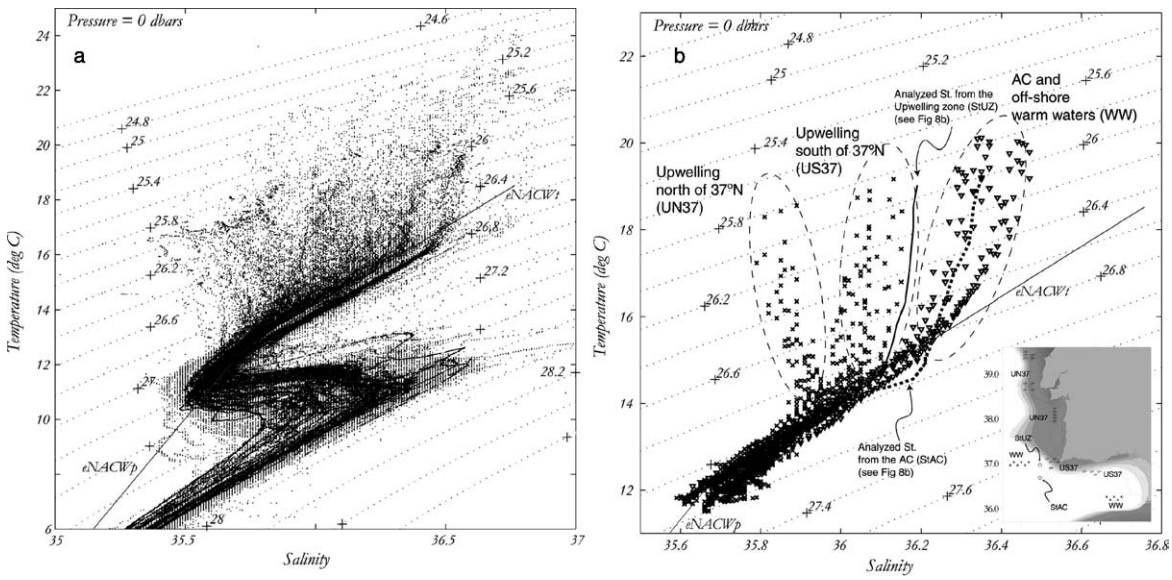

Figure 5. (a) Temperature–salinity (T–S) scatter plots of the historical data set. (b) T–S scatter plots of selected groups of stations along the coast of SW Portugal: (i) upwelling stations (crosses) north of 37°N (UN37) and south of 37°N (US37); (ii) (triangles) Azores current and warm offshore waters (WW); (iii) (bold line) analysed offshore station under the influence of the upwelling (StUz); (iv) (dashed line) analysed offshore station under the influence of the Azores current (StAC). Groups of stations are circled for clarity. The spatial location of selected stations is shown in the inset of (b).

Thermohaline characteristics of the Azores current are also observed below the thermocline (Figure 6c and d). At subsurface levels O(150–200) m smaller-scale extensions of the upwelled region are observed to stretch towards the oceanic zone thus featuring a number of contortions of the thermohaline front. Offshore ejections of low-salinity (35.94–35.98) and colder (13.6–14°C) water seem to be injected into the exterior ocean. The appearance of a number of offshore prolongations of the upwelling water should be noted; they are marked with arrows in Figure 6d. The loci of these occurrences are closely linked to the main capes; namely south of 38°N (Cape Roca), associated with the Cape St. Vincent and the third one at 8°W in the vicinity of Cape St. Maria.

Below 300 m there is no obvious indication of the Azores current and the upwelling signal weakens. At 400 m a wedge of warm (>12.0°C) and saline (>35.7) water invades the continental slope of the Gulf of Cadiz (Figure 6e and f). This strongly contrasts with the situation at shallower levels, with more saline waters offshore. The plume has features compatible with the definition of a shallow core of MOW from a subdivision of the "upper core" due to topographic effects in the Gulf of Cadiz that have already been traced along the Portuguese upper continental slope of the IP (Ambar, 1983).

The movement of surface waters in relation to the eNACW line is also of interest. T–S scatter plots of some analysed stations are presented in Figure 5b. These correspond to the upwelling areas at both the west and south coasts, and to the warm offshore zone under the influence of the Azores current (see location in the inset of Figure 5). Coastal upwelling waters are colder and less saline than both offshore waters and waters with AC influence. The graph shows the differential T–S properties of upwelled waters south and north of 37°N. The former may be subjected to a variable degree of mixing between the waters upwelled north of 37°N and AC waters.

Dynamic height and geostrophic velocity structure

Dynamic topography and geostrophic velocities at 10 m with reference to the 400-m reference level are presented in Figure 7. Cross-sections of geostrophic velocities are presented in Figures 8 and 9 together with thermohaline fields. Geostrophic-velocity values shown here are generally low. Hinrichsen and Lehmann (1995) observed that geostrophic currents and directly measured velocity in the Iberian Basin showed good correlation in direction but not in magnitude. The unsolved problems of the "level of no motion", viz. first, small-scale perturbations and ageostrophic components that occur in regions of sloping bottom topography and second, inertial and semidiurnal tidal currents that are unaccounted for in the geostrophic approximation, may bias indirect current measurements by about ± 10 cm s^{-1}. In spite of the climatological averaging these effects are expected to be considerable near Cape St. Vincent and in the Gulf of Cadiz (Hinrichsen and Lehmann, 1995). Furthermore, the averaging method reduces horizontal variability and smoothes the climatological geostrophic values with respect to synoptic measurements.

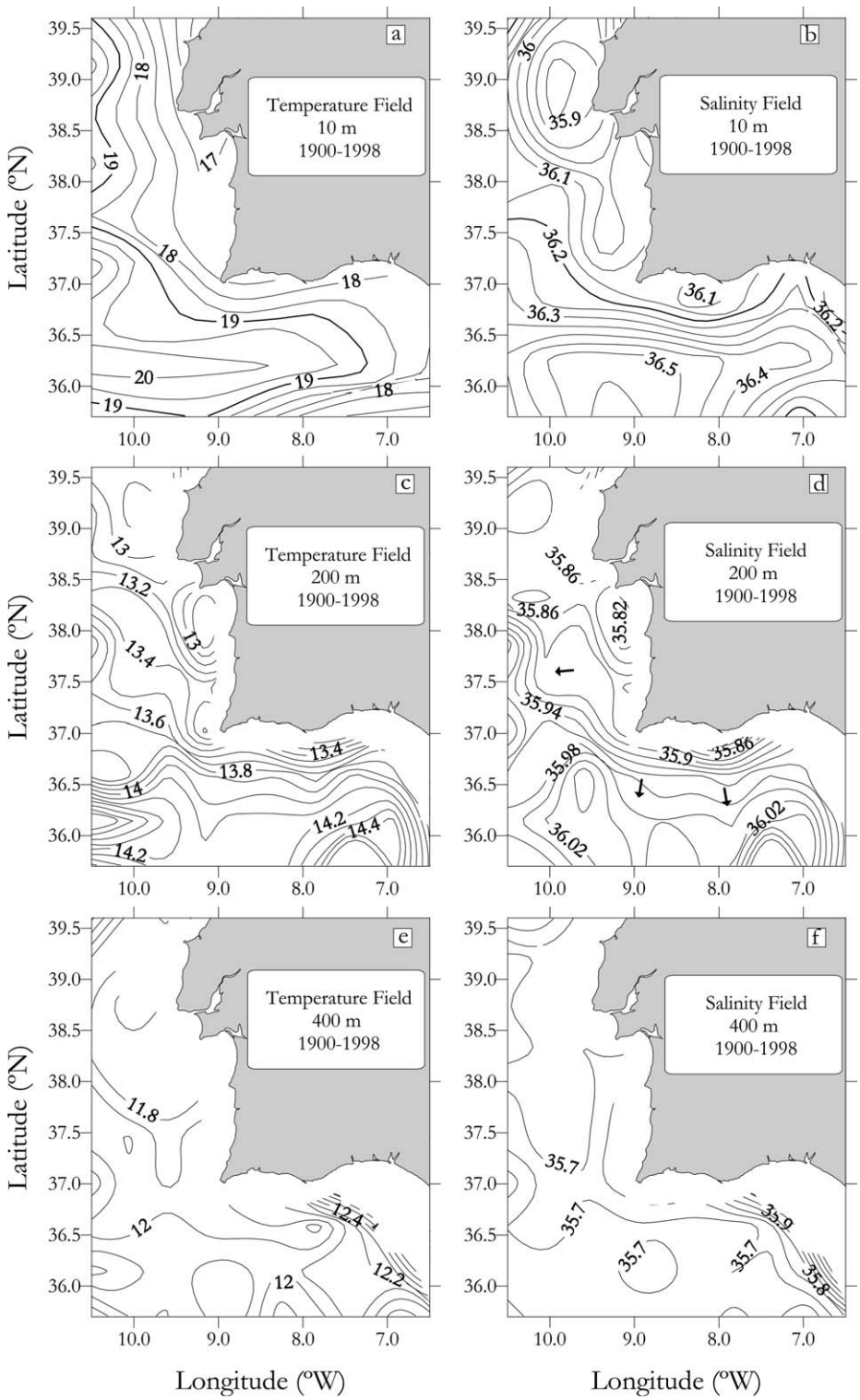

Figure 6. Temperature (°C) and salinity, respectively, at: (a) and (b) 10 m; (c) and (d) 200 m; (e) and (f) 400 m. The 30 m (a and b), 200 m (c and d) and 500 m (e and f) bathymetric contours are also shown. The arrows in (d) highlight the offshore projections of the upwelling zone.

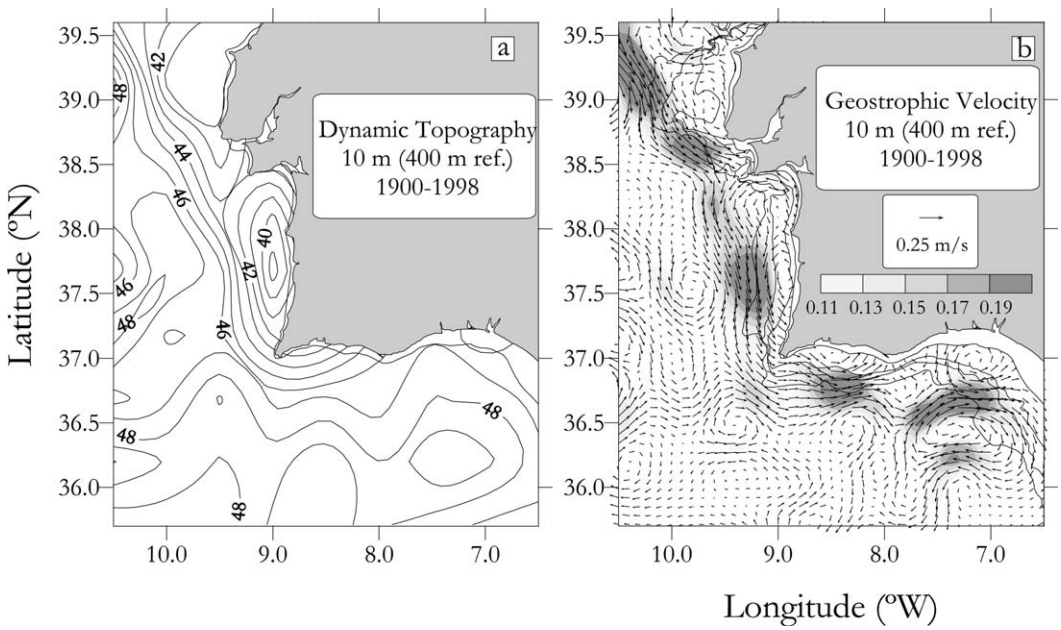

Figure 7. (a) The dynamic topography in dynamic cm at 10 m (400-m reference level). (b) The geostrophic velocity vectors at 10 m. Shades and contour scale indicate the module of geostrophic velocity. The 30 and 100 m bathymetric contours are also shown.

Low dynamic-height values are observed along the coastal upwelled area with higher values offshore (Figure 7a). Along the main dynamic front an upwelling jet develops, separated from the coastline and parallel to the shelf break conveying the cold and low-salinity water equatorward. A number of meanders spatially coincide with offshore extensions of the upwelling fringe described earlier. The upwelling jet bends cyclonically off Cape Roca and proceeds equatorward slightly approaching the coast following the bathymetry until 37°30′N where it seems to experience an offshore meander before it bends around Cape St. Vincent. On the southern shelf the front also follows the bathymetry, yet it seems to have two major ejections: the first, south of Cape St. Vincent, and the second, off Cape St. Maria. Maximum geostrophic-velocity values of approximately 16–22 cm s^{-1} are observed at 37°30′N for the upwelling jet (Figure 7b). The climatological Azores current is a coherent eastward flow centred at 36°30′N, with maximum velocity ∼7 cm s^{-1}. When this flow encounters the upwelling jet it seems to partially merge with the equatorward flow while the remainder is deflected northwards as an offshore countercurrent, with maximum velocities of about 10 cm s^{-1}. Downstream cyclonic cells at the main capes are found. The most conspicuous of these is found south of Cape Roca, where the feature is intense and coherent. It is responsible for a return flow inshore of the upwelling jet. A weaker cyclone is observed east of Cape St. Maria, which notably coincides with the existence of counterflows along the northern shelf of the Gulf of Cadiz (Relvas and Barton, 2002). Cyclonic flow also characterizes the region downstream of Cape St. Vincent. Offshore southeastwards of Cape St. Maria a large anticyclone seems to be anchored in the Gulf of Cadiz and this closes the anticyclonic loop along the southern region.

Warmer and more saline waters occupy the offshore region throughout whereas upwarping of isotherms and isohalines feature in the coastal region (Figure 8). Cold and particularly low-salinity waters typify the upwelling zone and are entrained by the equatorward flow. The analysis of the vertical structure of the baroclinic velocity and thermohaline properties following the upwelling jet at transects 37°30′N and 8°30′W shows that the path of the upwelling jet and that of the associated current system may be traced by its thermohaline properties, as could be observed from Figure 5b. The highest geostrophic-velocity values are surface-trapped, associated with the upwelling jet and always found in the upper 150 m. The inshore portion of these transects shows evidence of the presence of a countercurrent interior to the upwelling with velocities up to 8 cm s^{-1} off the west coast (Figure 8c and f).

Although most of the upwelling flow evolves parallel to the coast, the analyses of the thermohaline fields plus the velocity structure lead to evidence of some cross-shelf exchanges associated with offshore projections of the upwelling fringe (Figure 9). Their thermohaline features allow them to be traced back to the upwelling region. Their existence can be interpreted as episodic but repeated appearances of ejections of the upwelling front. These appear to be significantly linked to the most prominent capes, namely Cape Roca, Cape St. Vincent and Cape St. Maria. Along transect 09°30′W and centred at ∼37°12′N an offshore projection of the upwelling jet is clearly

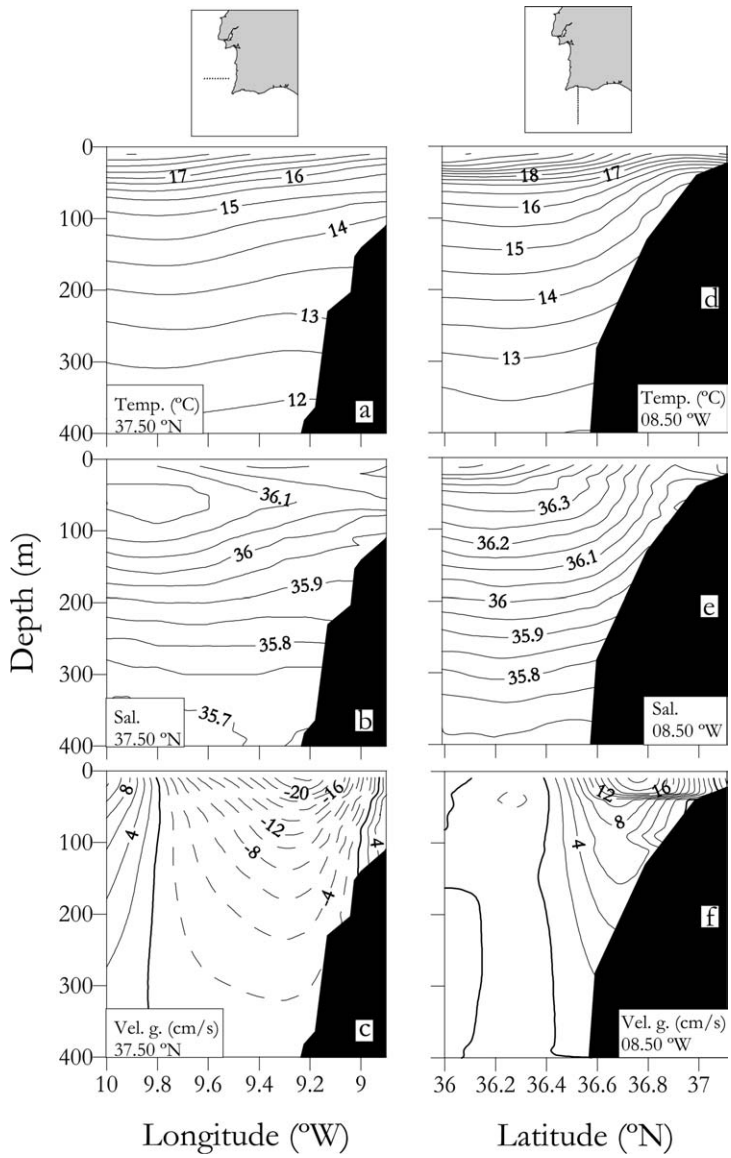

Figure 8. Cross-shelf transects of temperature (°C), salinity and geostrophic velocity (cm s^{-1}) across 37°30′N (a–c) and across 08°30′W (d–f). Dashed lines in (c) and (f) indicate negative (southward and westward) geostrophic velocities.

observed as a cold and low-salinity signal, at both sides of which partial re-circulations are inferred (Figure 9a–c). Likewise on the southern tip along transect 36°30′N two of these meanders seem to be associated with partial re-circulations of the upwelled water. These appear centred at 9°W and 8°W as shown in Figure 9d–f.

Cross-shelf exchanges seem particularly enhanced in the vicinity of Cape St. Vincent. They leave conspicuous prints in the thermohaline and dynamic fields both west and south of the Cape. A subsurface signal associated with the upwelling jet seems to draw recurrent excursions of the upwelling front during the period under review on both sides of the Cape (marked with arrows in Figure 9e). These may eventually break out in the form of upwelling filaments, like those off Cape St. Vincent, which have been extensively studied with AVHRR satellite imagery (Relvas and Barton, 2002).

Volume transport estimates

Volume transports have been calculated from the historical data set (Figure 10). Figure 10a represents the geostrophic transport function at 10 m over the 400-m reference level. The component of the geostrophic transport normal to the

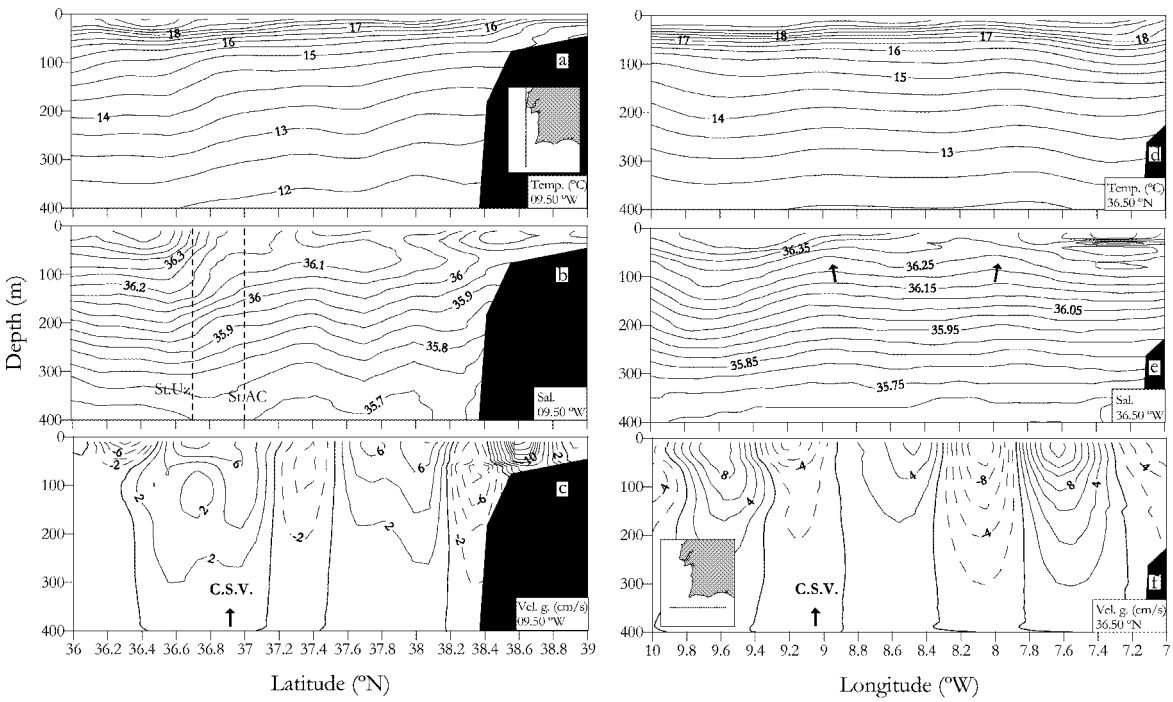

Figure 9. Along-shelf transects of temperature (°C), salinity and geostrophic velocity (cm s^{-1}) across 09°30′W (a–c) and 36°30′N (d–f). The dashed lines in (c) and (f) indicate negative (southward and westward) geostrophic velocities. C.S.V. indicates Cape St. Vincent. The arrows in (e) mark the uplift of the isohalines following the offshore projection of the upwelling front. The dashed vertical lines in (b) point to the locations where T–S plots corresponding to the analysed offshore stations influenced by the Azores current (StAC) and the coastal upwelling (StUz) have been depicted (see Figure 5b).

cross-sections is plotted in Figure 10b–e. Units are Sverdrups (1 Sv = 10^6 m^3 s^{-1}). A schematic view with the interpretation of the general circulation may be seen in Figure 11. For the 10–400-m layer anticyclonic circulation over the CTZ is the main feature. The equatorward stream conveys ∼1 Sv parallel to the coastline. The larger-scale circulation pattern is formed by an equatorward, partially separated, coastal flow and a coherent, offshore poleward movement although cross-shelf circulations in both the offshore ocean area and the neritic zone bring about considerable mass exchanges. In climatological terms the most vigorous of these exchanges are observed in the vicinity of Cape St. Vincent, where the upwelling jet exports half of the flow offshore, before a similar amount is incorporated from the Azores current. After turning round the Cape the equatorward flow has partial cross-shelf re-circulations of O(0.30) Sv with the offshore current system. East of 8°30′W most of the flow diverts offshore again to return coastwards and follow the bathymetry (Figure 11). It could be argued that part of this stream may turn anticyclonically to the Gulf of Cadiz and form the offshore poleward flow that transports ∼0.6 Sv. In areas other than that of Cape St. Vincent a small part of the flow of 0.10 ± 0.01 Sv appears to proceed polewards over the shelf area inside the upwelling jet as a coastal countercurrent (e.g. Figure 10b).

Discussion

Many authors have attempted to understand the circulation along the IP zone with the aid of numerical models (e.g. Batteen *et al.*, 2000; Coelho *et al.*, 2002), satellite imagery (e.g. Stevenson, 1977; Fiúza, 1983; Folkard *et al.*, 1997; Relvas and Barton, 2002), *in situ* observations (e.g. Frouin *et al.*, 1990; Haynes and Barton, 1990; Haynes *et al.*, 1993) and volume budgets and box calculations from synoptic surveys (e.g. Baringer and Price, 1997; Mazé *et al.*, 1997; Mauritzen *et al.*, 2001). From infrared imagery and *in situ* data the early work of Stevenson (1977) established some of the main features found in this spring–summer climatological analysis. This author inferred generalized anticyclonic circulation in the Gulf of Cadiz separated from a warm coastal countercurrent in the eastern Gulf of Cadiz by an ocean front that he called the Huelva Front. Additionally he also cited offshore projections of the upwelled water in the Cape St. Maria area, where strong velocity shears were inferred (e.g. the Stafford shear). Fiúza (1983) and Folkard *et al.* (1997) linked these characteristic surface circulation patterns as inferred from satellite SST data with the local wind regime.

From the present analysis the equatorward spring–summer transport of low-salinity, cold, upwelled waters by the upwelling jet into the Gulf of Cadiz has been

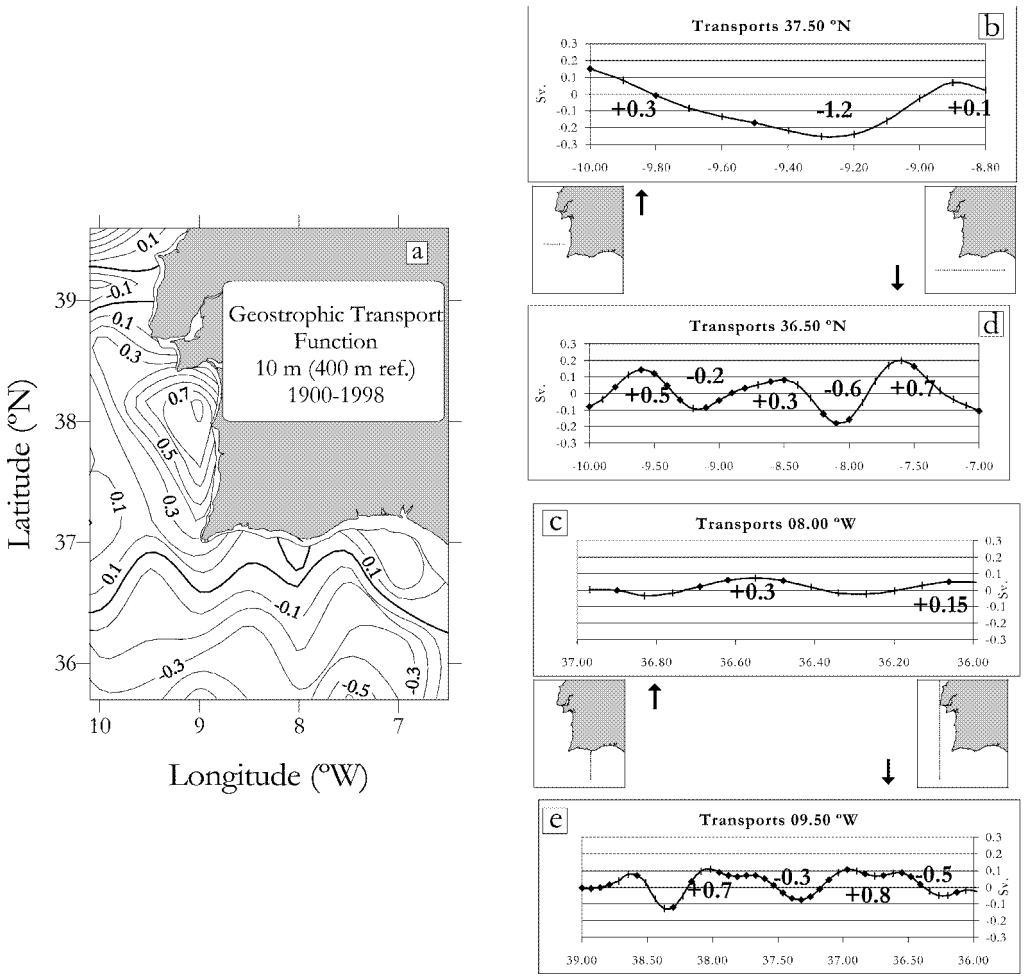

Figure 10. (a) The geostrophic transport function at 10 m (400-m reference level). The units are Sverdrups (1 Sv = 10^6 m^3 s^{-1}) and the line interval is 0.1 Sv. (b) The geostrophic transport across 37°30′N integrated over 10–400 m. (c) As in (b) but across 08°00′W. (d) As in (b) but across 36°30′N. (e) As in (b) but across 09°50′W.

estimated to be ∼1 Sv through the upper 400 m (Figure 11). Offshore, a warmer and more saline flow transports ∼0.4–0.6 Sv polewards. Inshore of the upwelling jet, a weaker cyclonic re-circulation is speculated. The climatological analysis has also revealed significant volume exchanges perpendicular to the shelf, the most significant ones west of Cape St. Vincent. There, the upwelling jet exports an important part of the transport (∼0.5 Sv) offshore in an anticyclonic flow. A smaller amount (∼0.1 Sv) is re-circulated inshore of the upwelling jet in a cyclonic cell. Both flows are seen as feeding both the inshore and the offshore countercurrents, and they are observed to join the equatorward flow at more northern locations. West of Cape St. Vincent the climatological Azores current and the upwelling jet merge, the former making ∼0.5 Sv available for the upwelling jet to continue eastwards and to turn around the Cape. In the southern area, east of 8°30′W off Cape St. Maria significant exchanges are caused by a well-defined contortion of the upwelling front.

Individual synoptic cruise data show agreement with the climatological circulation features. First, data from the cruise 201 of R/V "Poseidon", leg 9 (POS 201/9) performed between 11 and 22 June 1994 during weak upwelling winds (Relvas and Barton, 1996) are presented in Figure 12. The picture in 1994 was generally similar to the climatological circulation, with a well-developed upwelling jet flowing over the slope and separated from the shelf by a coastal countercurrent. Offshore, a poleward flow closed the three-stripped pattern of the SW Portugal current system. Transport estimates have been calculated from acoustic Doppler current profiler (ADCP) velocities over the 16–400-m layer (Figure 12). Volume transport associated with the inshore countercurrent increased from 0.35 Sv at 37°6′N to 0.98 Sv across 37°36′N. This

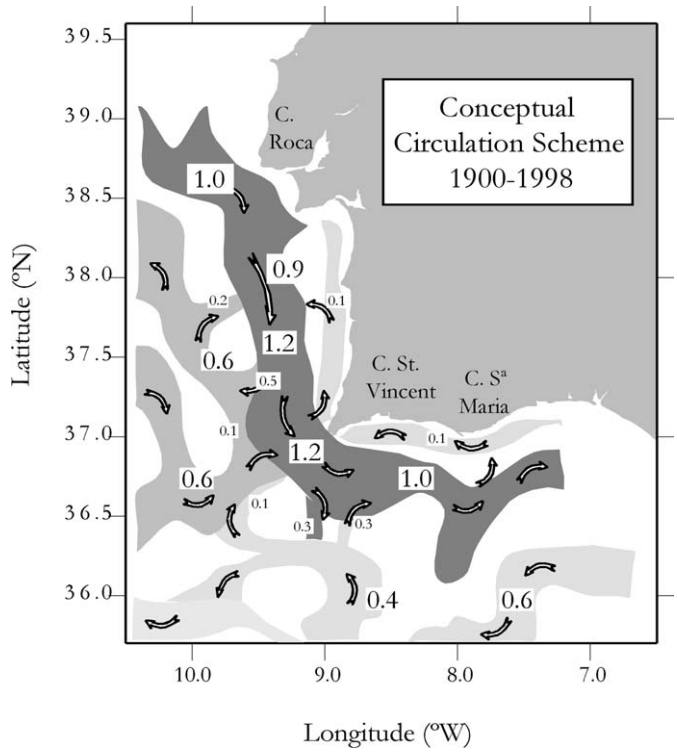

Figure 11. A schematic view of the spring–summer flow system along the southwestern Portuguese coast; volume transports (units are Sv) are labelled; dark tones represent the cold, lower-salinity, equatorward current.

increment was accompanied by a similar decrease in volume transport associated with the upwelling jet, which dropped from 1.87 Sv at 37°36′N to 1.26 Sv across 37°6′N. It is reasonable to consider the hypothesis of northward re-circulation of ∼0.6 Sv in a cyclonic loop inshore of the upwelling jet. Such features could also be inferred from the historical data set (cf. Figure 8c and f). Direct observations taken in June 1994 reinforce the existence of an important mechanism of coastal re-circulation and poleward transport of ∼80% of the equatorward flow inshore of the upwelling jet along the western Portuguese coast, at least under relaxation of upwelling-favourable winds.

The joint SESITS 98 P and SESITS 98 S cruise, performed with the R/V "Noruega" (IPIMAR, Portugal) and R/V "Coornide de Saavedra" (IEO, Spain) between 31 October and 11 November 1998 sampled with a CTD an upwelling situation using a mesoscale-resolving scheme (SESITS, 1999) (Figure 13). The wind was blowing vigorously from the north along the west coast throughout the cruise (not shown). This cruise was conducted in the autumn and therefore it was not included in the climatological data set. Two westward-extending, filament-like features were sampled (Figure 13a), which showed both temperature and salinity anomalies (not shown). This suggests that they had been advected offshore from the coastal upwelled zone. The first large offshore excursion of upwelled water occurred off Cape Roca and the second off Cape St. Vincent. Both showed asymmetry in satellite SST signature, with stronger thermal gradients (>2.0°C over 10 km) on the southward flank than on their northward side. The satellite image is not shown but is structurally identical to the temperature distribution at 10 m in Figure 13a. The Cape Roca filament showed offshore and onshore geostrophic velocities of ∼20 cm s^{-1}. A finer spatial scheme of stations off Cape St. Vincent allowed the calculation of onshore geostrophic velocities >22 cm s^{-1}, showing that this value is highly dependent on the sampling design. In both cases the baroclinic volume transport re-circulated after the offshore excursion in a sharp meander, and was approximately 0.5–0.7 Sv over the 10–400-m layer (Figure 13b). The fact that these structures play a significant role in terms of the advection or retention of planktonic material and their subsequent relationship with the recruitment of commercial fish stocks over SW Portugal in autumn are well known (SESITS, 1999).

Seasonal volume transport calculations across selected transects on the west coast (37°–38°N) and the south coast (9°–7°W) have been retrieved from the literature and the historical database (Figure 14 and Table 1). The computation method is referred to in Table 1. Few of the data were obtained after box calculations. There is a large amount of baroclinic transport as depicted in the table. Most of transport estimates are comparable in magnitude and bounded by the values 1.7 Sv poleward −1.4 Sv equatorward. However,

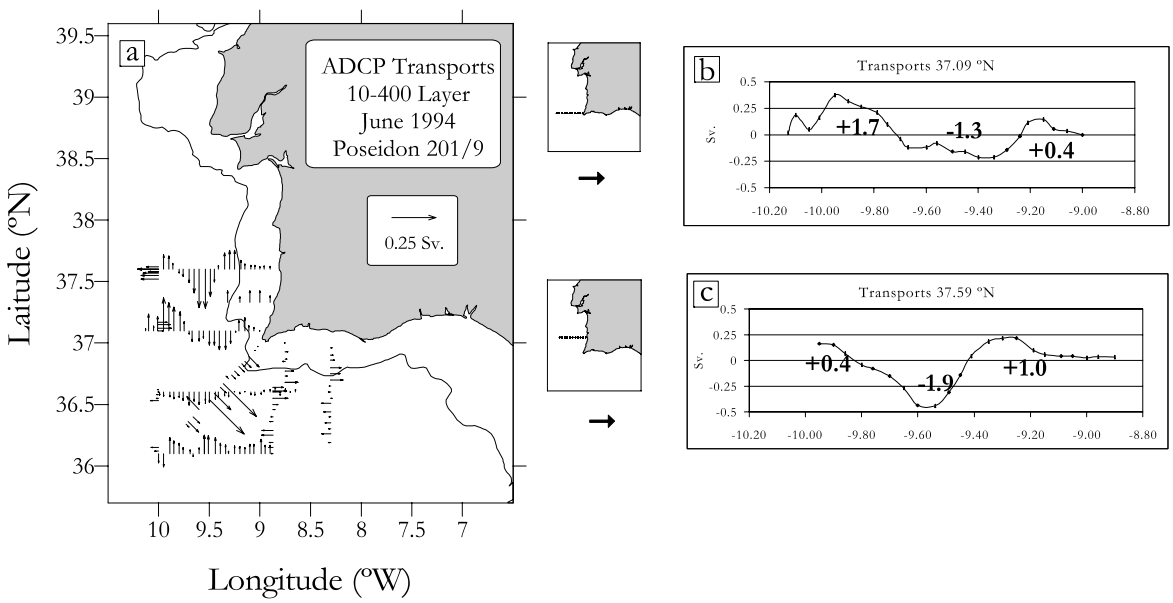

Figure 12. June 1994 ADCP volume transports. (a) Top view of the transports integrated from 10 to 400 m. The 500 m bathymetric contour is shown. (b) Transports across 37°09′N integrated over 10–400 m. (c) As in (b) but across 37°59′N. The volume transports (units are Sv) are labelled.

they are small compared with the values obtained by Mazé *et al.* (1997). However, these authors observed that the "reference level problem" could be responsible for their high transport and so their results have not been used in Figure 14. The seasonal pattern shows that the most intense equatorward transport occurs in spring–summer (between 0.7 and 1.3 Sv) when the poleward flow falls to its seasonal minimum. In autumn–winter, on the other hand, the equatorward transport weakens and the poleward flow peaks, with values up to 1.4–1.5 Sv in November–January. As a result, the net transport switches from approximately 0.5 Sv equatorward in spring–summer to about 0.5 Sv poleward in winter.

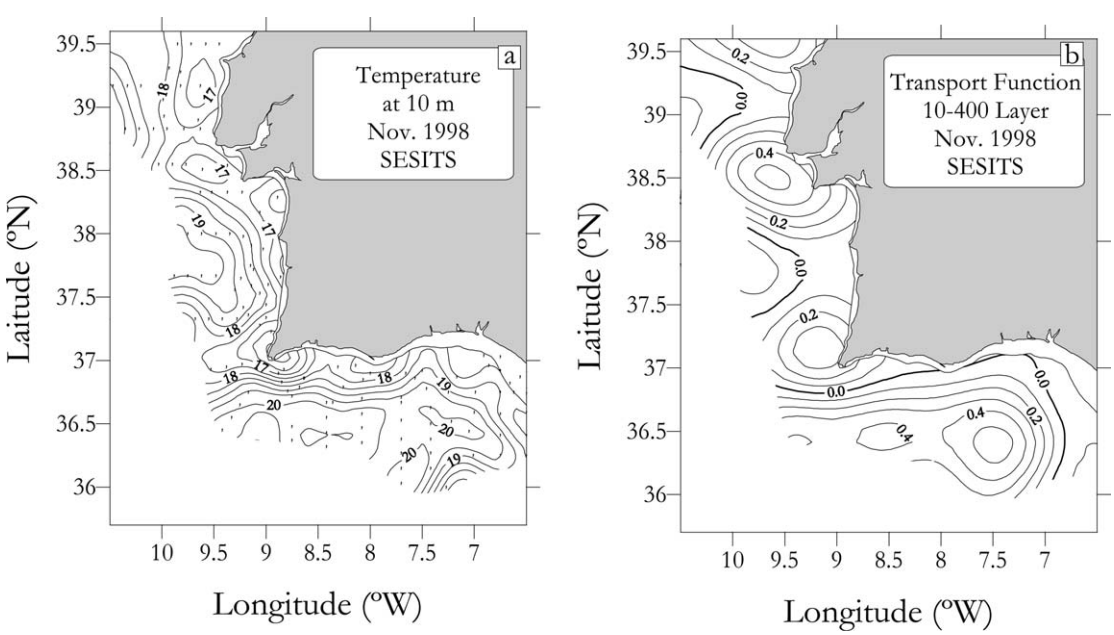

Figure 13. November 1998. (a) Temperature (°C) at 10 m. The 30-m bathymetric contour is shown. (b) Top view of geostrophic-transport function at 10 m (400-m reference level). Units are Sv. Line interval is 0.1 Sv.

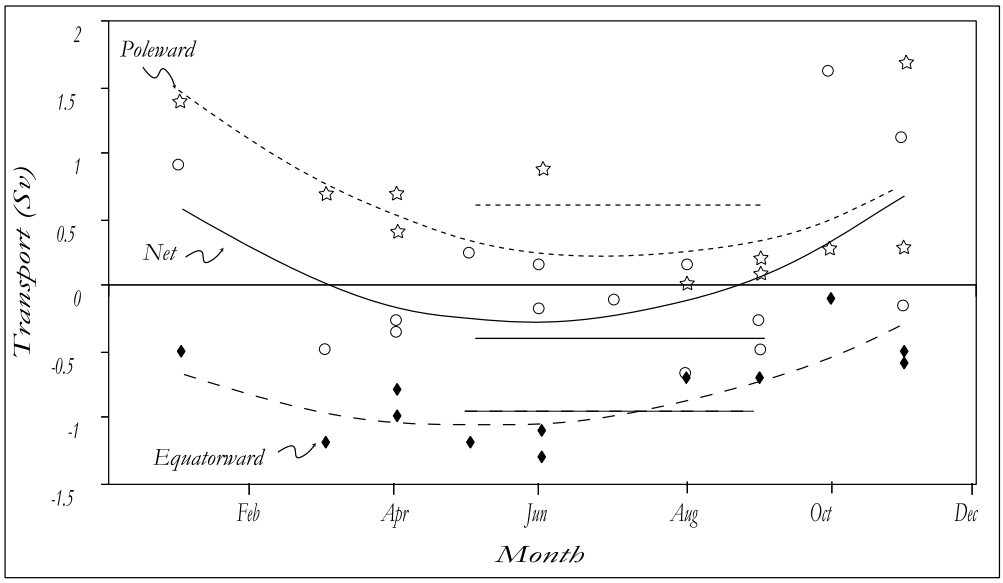

Figure 14. Annual, alongshore volume transport off SW Portugal according to Table 1. Poleward transport is plotted as asterisks, equatorward transport is plotted as filled diamonds and net transport is plotted as circles. Parabolic fits are drawn. The values are retrieved from the historical database and from the reviewed literature. Each data source is indicated in Table 1. There are more "net" data than detailed poleward/equatorward contributions and hence "net" transport does not necessarily indicate "poleward + equatorward". Spring–summer climatological values calculated in the present paper are also depicted as straight lines.

What is the role of the equatorward flow in terms of the oceanography of the Gulf of Cadiz? The literature refers to a general eastward drift of eNACW entering the Gulf of Cadiz. In this sense, Baringer and Price (1997) consider that the Atlantic inflow into the Gulf of Cadiz (from the surface to 27.0 sigma-t) is well balanced with the Atlantic inflow into the Mediterranean Sea (~1 Sv) and downward entrainment (i.e. progressive admixing at lower layers) within the MOW (~2 Sv). However, the most recent results point out that there is excess of Atlantic water in the Gulf of Cadiz. Mazé *et al.* (1997) calculated volume transports of 1.2 Sv southwards and 4.9 Sv northwards in the eNACW layer (from the surface to 27.25 sigma-t, with variable depth from 300 to 600 m) across 37°N west of Cape St. Vincent inshore of 10°W in May 1989. The authors concluded that there was a seasonal supply from the west Portugal region into the Gulf of Cadiz (the upwelling jet), but from budget calculations they inferred an additional source of eNACW elsewhere. This could be supplied by either the Azores current (Johnson and Stevens, 2000) or by other flows coming from southern latitudes or a mixture of both sources. These options are considered in turn below.

The influence of the Azores current was noted earlier in the present climatological analysis. The salinity transect along 9°30′W shows that the climatological eastward transport south of 37°6′N is a two-core structure (Figure 9b–c). A T–S plot is constructed with two analysed stations at the points marked with a dashed line in Figure 9b (see Figure 5b). The branch centred at 37°N is associated with water upwelled on the west coast (note also the uplift of the isotherms–isohalines in Figure 9a–b), which is made available to feed a prolongation of the jet along the southern coast, or to join waters locally upwelled on the southern flank in an eastward flow. It was observed that these waters may eventually also be the source of inshore re-circulations north of 37°N (see Figure 11). The secondary branch at 36°42′N advects warmer and saltier waters eastwards. These waters must have their origin at more westerly longitudes and it is suggested that they form part of a branch of the Azores current that partially admixes with the upwelling flow into the Gulf of Cadiz. Merging of both currents was already pointed out by Lozier *et al.* (1995). These authors mapped the climatological Azores current as a southeastward-extending branch of the NAC that extends well beyond 20°W. They discussed the observed convergence of a flow, presumably the Portugal current, into the AC from the northwest at the surface (26.5–27.0 sigma-t surfaces ±50–300 m) in the vicinity of the IP.

With regard to the second possible source, Mauritzen *et al.* (2001) computed zonal volume transport from 9°W south of Cape St. Vincent to the African coast in November 1958, based on a reference level at the salinity minimum. For their preferred EXP2 solution, the main inflow occurred along the African coast. There was also an indication of northward boundary-current circulation within the Gulf of Cadiz, with 1.7 Sv westward transport from the coast to 36°30′N and 0.6 Sv eastward from 36°30′ to 36°N. These results support the

Table 1. The annual, alongshore volume transport off SW Portugal. Date, source, section, data type, method, reference level and bibliographic reference are also indicated.

Date	Source	Section	Poleward transport (Sv)	Equatorward transport (Sv)	Net transport (Sv)	Data type	Method	Layer (reference level)	Bibliographic reference
January 1974	NODC	37.5	1.4	−0.5	0.9	CTD	Geostrophy	10–400	?
March 1996	NODC	7	0.7	−1.2	−0.5	CTD	Geostrophy	10–400	?
April 1974	NODC	37.6	0.4	−0.8	−0.4	CTD	Geostrophy	10–400	?
April 1988	NODC	7	0.7	−1	−0.3	CTD	Inv. Mod	10–400	Baringer and Price (1997)
May 1988	BORD-EST	37.5	N/A	N/A	0.23	CM	Currentometry	150–450	Arhan *et al.* (1994); Coelho *et al.* (2002)
May 1989	BORD-EST	37	4.9	−1.2	3.7	CTD	Inv. Mod	27.25	Mazé *et al.* (1997)
June 1994	EURO-SQUID	37	0.9	−1.1	−0.2	CTD	Geostrophy	10–400	Relvas and Barton (1996)
June 1994	EURO-SQUID	37	N/A	−1.3	N/A	ADCP	ADCP	10–400	Relvas and Barton (1996)
June 1988	NODC	37.5	N/A	N/A	0.13	CM	Currentometry	150–450	Arhan *et al.* (1994); Coelho *et al.* (2002)
July 1988	NODC	37.5	N/A	N/A	−0.1	CM	Currentometry	150–450	Arhan *et al.* (1994); Coelho *et al.* (2002)
August 1974	NODC	37.6	0	−0.7	−0.7	CTD	Geostrophy	10–400	?
August 1988	NODC	37.5	N/A	N/A	0.15	CM	Currentometry	150–450	Arhan *et al.* (1994); Coelho *et al.* (2002)
September 1991	WOCE	37	0.2	−0.7	−0.5	CTD	Geostrophy	10–400	WOCE
September 1992	WOCE	8	0.1	−0.4	−0.3	CTD	Geostrophy	10–400	WOCE
September 1988	NODC	37.5	N/A	N/A	0.56	CM	Currentometry	150–450	Arhan *et al.* (1994); Coelho *et al.* (2002)
October 1973	NODC	37	0.3	−0.1	0.2	CTD	Geostrophy	10–400	?
October 1988	NODC	37.5	N/A	N/A	0.46	CM	Currentometry	150–450	Arhan *et al.* (1994); Coelho *et al.* (2002)
October 1995	NODC	36.3	N/A	N/A	1.6	ADCP	ADCP	Sal min	Cherubin *et al.* (1997); Mauritzen *et al.* (2001)
November 1998	SESITS	37.3	0.3	−0.5	−0.2	CTD	Geostrophy	10–400	SESITS (1999)
November 1958	IGY	9	1.7	−0.6	1.1	CTD	Inv. Mod	Sal min	Swallow (1969); Mauritzen *et al.* (2001)
Summer 1900–1998	NODC	37	0.6	−1	−0.4	CTD	Geostrophy	10–400	This paper

work of Iorga and Lozier (1999), who hypothesized that the climatological IPC could have its origin further south along the African coast.

More shallow Atlantic water moves eastward than is needed for entrainment in the Gulf of Cadiz and dense water formation in the Mediterranean Sea (Mauritzen *et al.*, 2001). Budget calculations call for a compensatory, return-poleward flow exporting the excess mass off the Gulf in the upper layers. The shallow Atlantic water must show a tendency for re-circulation and to spread the Atlantic water (with its increased salinity) westwards above the MOW on the northern side of the Gulf of Cadiz in a so-called detrainment process (Mauritzen *et al.*, 2001). There are enough pieces of evidence of winter poleward flow along the western IP (e.g. Frouin *et al.*, 1990; Haynes and Barton, 1990). Summer poleward flow has been observed recently off southwestern Portugal (Relvas and Barton, 2002) and along the northern flank of the Gulf of Cadiz (Stevenson, 1977; Fiúza, 1983; Folkard *et al.*, 1997) as inshore, poleward countercurrents at times of upwelling relaxation. Data from June 1994 revealed that this transport may be important under weak upwelling conditions, and that it can reach up to 1 Sv. Quantitative estimates in the present climatological study fail to fully represent the inshore poleward transport. Since the low-pass smoothing filter cuts off features below 70-km size, the smaller mesoscale features of the order of the baroclinic radius of deformation (∼25 km for the region) such as the nearshore countercurrent should be either smoothed or filtered out by the analysis. The inshore region is dominated during upwelling relaxations by westward flow along the coast as a non-geostrophic response of the alongshore pressure gradient existing along the SW Portuguese coast (Relvas and Barton, 2002 and cf. Figure 7a). Direct observations (June 1994, Figure 12) suggest strong transport associated with this inshore countercurrent. Bedform records support

this oceanographic pattern: seismic analysis (Lobo *et al.*, 2003) points out two opposing patterns of sediment dispersal in the northern Gulf of Cadiz, with eastward transport on the middle to outer shelf, and westward dispersal in the inshore zone.

The hydrographic and velocity plots in Figure 9d–f show large meanders of the upwelling jet in the vicinity of the Cape St. Vincent and Cape St. Maria, as featured by a subsurface upward doming of the isohalines, marked with arrows in the figure. Relative maxima of salinity and temperature are centred along both sides of this jet, thus strengthening the density gradients (not shown). Cross-shelf exchanges of O(30%) of the coastal jet are observed south of the Cape St. Vincent (Figure 11). This transport is interpreted as products of the averaging of recurrent extensions of the upwelling jet, in the form of the Cape St. Vincent filament, over the period of study. The meander of the equatorward flow observed in the vicinity of Cape St. Maria may be associated with the coastal separation imposed by the penetration of the upwelling jet onto a region with an opposed regime (Relvas and Barton, 2002). Similar meanders have been observed in the coast of California (Barth *et al.*, 2000).

Conclusions

Atmosphere–ocean interaction through Ekman mechanisms plays a key role in the definition of the upper circulation pattern off the southwest of the IP. Climatological wind data analysis reveals the seasonal dependence of the upwelling and associated circulation. From May to September the Ekman layer is divergent in the Iberian CTZ.

Although alongshore transports dominate the circulation pattern of the upper layers, cross-shore transports are significant and are recognized at the climatological scale. The spring–summer climatological circulation is dominated by an equatorward flow of relatively cool and low-salinity water associated with the upwelling regime induced by a favourable wind pattern. This flow conveys about 1 Sv parallel to the bathymetry and is partially separated from the coast. Offshore, a warmer and more saline flow transports ~0.4–0.6 Sv polewards. Interaction between both flows results in an anticyclonic circulation with an exchange of ~0.5 Sv to the offshore poleward flow and the partial re-circulation further north, into the equatorward flow. Inshore of the upwelling jet, a weaker cyclonic re-circulation is speculated and justified on the basis of synoptic data. In the light of these results the shelf break may be seen as a climatological border on both sides of which two major re-circulation cells occur, at least at the climatological scale.

Part of the equatorward upwelling jet turns eastwards around Cape St. Vincent to satisfy potential vorticity conservation. In this area, a significant transport from the Azores current (O(0.5) Sv) is incorporated into the upwelling jet that conveys ~1.2 Sv across Cape St. Vincent, then flows eastwards along the southern coast and possibly mixes with locally upwelled waters. The equatorward flow has partial cross-shelf re-circulations of O(0.30) Sv along the southern coast, with inferred interactions with the offshore current system. Across 8°42′W the upwelling jet again proceeds parallel to the southern coast carrying ~1 Sv.

Major exchanges between both current systems are related to the abrupt changes of the coastline. The climatological offshore protrusions of the equatorward flow are interpreted as recurrent episodes of major contortions of the upwelling flow, namely upwelling filaments. These features may bring about considerable cross-shelf transport that can amount to 50% of the main flow. The most significant of these are found to be associated with Cape St. Vincent, where the upwelling front seems to stretch to both the west and south. The boundary discontinuity forces part of the equatorward jet to feed a major filament that stretches from it. Preferential zones for filament development identified in the literature were presented here from hydrographic analysis of the historical database. It can be concluded that these oceanographic features leave a "footprint" on the climatic cross-shelf transports in spite of the strong averaging-out of recurrent events over the spring–summer of 1900–1998.

East of 8°30′W offshore ejection of the upwelling jet in the form of a large meander following the bathymetry is observed off Cape St. Maria. Direct velocity observations presented here show inshore northward transport of the same order of magnitude as the upwelling jet. Purely topographically induced mechanisms partially explain the separation of the coastal jet. However, its penetration onto a region with an opposed flow regime seems to be a major mechanism for the separation, forcing the eastward flow of cold waters to develop in a conspicuously long, cold plume that spreads offshore in the vicinity of Cape St. Maria and beyond.

Acknowledgements

The present work was funded by CIMA-UAlg and ATOMS project (FCT contract PDCTM/P/MAR/15296/1999). We are indebted to the Chief Scientists of the EUROSQUID and SESITS projects. Three anonymous referees provided useful comments on an earlier version of the manuscript. Special thanks to Brad Morris for his valuable suggestions.

References

Ambar, I. 1983. A shallow core of Mediterranean water off western Portugal. Deep-Sea Research, 30(6A): 677–680.

Arhan, M., Colin de Verdière, A., and Memery, L. 1994. The eastern boundary of the subtropical North Atlantic. Journal of Physical Oceanography, 24: 1295–1316.

Bakun, A., and Nelson, C. S. 1991. The seasonal cycle of wind-stress curl in subtropical eastern boundary regions. Journal of Physical Oceanography, 21: 1815–1834.

Baringer, M. O., and Price, J. F. 1997. Mixing and spreading of the Mediterranean outflow. Journal of Physical Oceanography, 27(8): 1654–1677.

Barnes 1964. A technique to maximize details in numerical weather-map analyses. Journal of Applied Meteorology, 3: 396–409.

Barth, J. A., Pierce, S. D., and Smith, R. L. 2000. A separating coastal upwelling jet at Cape Blanco, Oregon and its connection to the California current system. Deep-Sea Research II, 47: 783–810.

Batteen, M. L., Martinez, J. R., Bryan, D. W., and Buch, E. J. 2000. A modelling study of the coastal eastern-boundary current system off Iberia and Morocco. Journal of Geophysical Research, 105(C6): 14173–14195.

Bormans, M., Garret, C., and Thomsom, K. 1986. Seasonal variability of the surface inflow through the Strait of Gibraltar. Oceanologica Acta, 3: 79–88.

Brink, K. H., Beardsley, R. C., Paduan, J., Limeburner, R., Caruso, M., and Sires, J. G. 2000. A view of the 1993–1994 California current based on surface drifters, floats and remotely sensed data. Journal of Geophysical Research, 105(C4): 8575–8604.

Chase, J. 1956. The Bermuda-Azores high pressure cell. Its surface wind circulation. *In* Miscelane Geofísica, pp. 29–54. Serviço meteorológico Nacional, Luanda.

Cherubin, L., Serpette, A., Carton, X., Paillet, J., Connan, O., Morin, P., Rousselet, R., Le Cann, B., Le Corre, P., Labasque, T., Corman, D., and Poete, N. 1997. Descriptive analysis of the hydrology and currents on the Iberian Shelf from Gibraltar to Cape Finisterre: preliminary results from the Semane and Interafos experiments. *Annales Hydrographiques*, 21: 5–81.

Coelho, H. S., Neves, R. J. J., White, M., Leitão, P. C., and Santos, A. J. 2002. A model for ocean circulation on the Iberian coast. Journal of Marine Systems, 32: 153–179.

Doswell, C. A. 1977. Obtaining meteorologically significant surface-divergence fields through the filtering property of objective analysis. Monthly Weather Review, 105: 885–892.

Enríquez, A. G., and Friehe, C. A. 1995. Effects of wind stress and wind-stress-curl variability on coastal upwelling. Journal of Physical Oceanography, 25: 1651–1671.

Fiúza, A. F. G. 1982. The Portuguese coastal-upwelling system. *In* Actual Problems of Oceanography in Portugal, pp. 45–71. Junta Nacional de Investigação Científica e Tecnológica, Lisbon.

Fiúza, A. F. 1983. Upwelling patterns off Portugal. *In* Coastal Upwelling, Pt. Ed. by A. E. Suess, and J. Thiede. Plenum Publishing Corporation, New York.

Fiúza, A. F. G., and Halpern, D. 1982. Hidrographic observations of the Canary Current between 21°N and 25.5°N in March/April 1974. Rapport et Proces Verbaux des Reunions. Conseil International pour l'Exploration de la Mer, 180: 58–64.

Fiúza, A. F. G., de Macedo, M. E., and Guerreiro, M. R. 1982. Climatological space and time variation of the Portuguese coastal upwelling. Oceanologica Acta, 5(1): 31–40.

Folkard, A. M., Davies, P. A., Fiúza, A. F. G., and Ambar, I. 1997. Remotely sensed sea-surface thermal patterns in the Gulf of Cadiz and the Strait of Gibraltar: variability, correlations, and relationships with the surface wind field. Journal of Geophysical Research, 102(C3): 5669–5683.

Frouin, R., Fiúza, A. F. C., Ambar, I., and Boyd, T. J. 1990. Observations of a poleward surface current off the coasts of Portugal and Spain during winter. Journal of Geophysical Research, 95(C1): 679–691.

Gill, A. E. 1982. Atmosphere–Ocean Dynamics. International Geophysics Series, Volume 30. Academic Press, Inc., New York. 662 pp.

Haynes, R. D., and Barton, E. D. 1990. A poleward flow along the Atlantic coast of the Iberian Peninsula. Journal of Geophysical Research, 95(C7): 11425–11442.

Haynes, R. D., Barton, E. D., and Piling, I. 1993. Development, persistence and variability of upwelling filaments off the Atlantic coast of the Iberian Peninsula. Journal of Geophysical Research, 98(C12): 22681–22692.

Hinrichsen, H. H., and Lehmann, A. 1995. A comparison of geostrophic velocities and profiling ADCP measurements in the Iberian Basin. Journal of Atmospheric and Oceanic Technology, 12: 901–914.

Huthnance, J. M. 1995. Circulation, exchange and water masses at the ocean margin: the role of physical processes at the shelf edge. Progress in Oceanography, 35: 353–431.

Iorga, M. C., and Lozier, M. S. 1999. Signatures of the Mediterranean outflow from a North Atlantic climatology. 1. Salinity and density fields. Journal of Geophysical Research, 104(C11): 25985–26009.

Johnson, J., and Stevens, I. 2000. A fine-resolution model of the eastern North Atlantic between the Azores, the Canary Islands and the Gibraltar Strait. Deep-Sea Research, 47: 875–899.

Krauss, W., and Käse, R. H. 1987. Mean circulation and eddy kinetic energy in the eastern North Atlantic. Journal of Geophysical Research, 89(C3): 3407–3415.

Large, W., and Pond, S. 1981. Open ocean momentum flux measurements in moderate to strong winds. Journal of Physical Oceanography, 11: 324–336.

Lobo, F. J., Sánchez, R., González, R., Dias, J. M. A., Hernández-Molina, F. J., Fernández-Salas, L. M., Díaz del Río, V., and Mendes, I. 2003. Contrasting styles of Holocene highstand sedimentation and inferred dispersal system on a sector of the Gulf of Cadiz shelf. Continental Shelf Research, in review.

Lozier, M. S., Owens, W. B., and Curry, R. G. 1995. The climatology of the North Atlantic. Progress in Oceanography, 36: 1–44.

Maddox, R. A. 1980. An objective technique for separating macroscale and mesoscale features in meteorological data. Monthly Weather Review, 108: 1108–1121.

Mauritzen, C., Morel, Y., and Paillet, J. 2001. On the influence of Mediterranean water on the central waters of the North Atlantic Ocean. Deep-Sea Research I, 48: 347–381.

Mazé, J. P., Arhan, M., and Mercier, H. 1997. Volume budget of the eastern boundary layer off the Iberian Peninsula. Deep-Sea Research I, 44(9/10): 1543–1574.

Nelson, C. S. 1977. Wind stress and wind-stress curl over the California current. NOAA Technical Report NMFS SSFR-714. U.S. Department of Commerce, Washington, DC. 87 pp.

NODC 2000. World Ocean Database 1998. Documentation and quality control. Version 2.0. Ocean Climatic Laboratory NODC Internal Report 14. Silver Spring, MD. January 2000 (URL: http://www.nodc.noaa.gov/oc5/pr_wodv2.html).

Nykjaer, L., and Van Camp, L. 1994. Seasonal and interannual variability of coastal upwelling along northwest Africa and Portugal from 1981 to 1991. Journal of Geophysical Research, 99: 14197–14208.

Ochoa, J., and Bray, N. A. 1991. Water–mass exchange in the Gulf of Cádiz. Deep-Sea Research, 38(Supplement 1): S465–S503.

Pingree, R. D. 1993. Flow of surface waters to the west of the British Isles and in the Bay of Biscay. Deep-Sea Research II, 40(12): 369–388.

Reid, J. L., and Mantyla, A. W. 1976. The effect of the geostrophic flow upon coastal-sea elevations in the northern Pacific Ocean. Journal of Geophysical Research, 81: 3100–3110.

Relvas, P., and Barton, E. D. 1996. Poseidon Cruise 201/9 Report: Acoustic Doppler Current Profiler Data ∼Velocity Fields. University of Algarve, Faro, Portugal. 51 pp.

Relvas, P., and Barton, E. D. 2002. Mesoscale patterns in the Cape São Vicente (Iberian Peninsula) upwelling region. Journal of Geophysical Research, 107(C10): 3164, (10.1029/2000JC000456).

Rodríguez, J. M., Hernandez-Leon, S., and Barton, E. D. 1999. Mesoscale distribution of fish larvae in relation to an upwelling

filament off Northwest Africa. Deep-Sea Research I, 46(11): 1969–1984.

Saunders, P. M. 1976. On the uncertainty of wind-stress-curl calculations. Journal of Marine Research, 34: 155–160.

Schlitzer, R. 2001. Ocean Data View (URL: http://www.awi-bremerhaven.de/GEO/ODV).

SESITS 1999. Evaluation of demersal resources of southwestern Europe from standardized groundfish surveys. Final Report to the Commission of European Communities. Contract Ref. DG XIV S.C. 96-029. 195 pp.

Smith, R. L. 1995. The physical processes of coastal ocean upwelling systems. *In* Zeithzchel Upwelling in the Ocean: Modern Processes and Ancient Records, pp. 39–64. Ed. by C. P. Summerhayes, K. C. Emeis, M. V. Angel, R. L. Smith, and B. Zeithzchel. John Wiley and Sons Ltd, London. 422 pp.

Stevenson, R. E. 1977. Huelva Front and Malaga, Spain, eddy chain as defined by satellite and oceanographic data. Deutsche Hydrographische Zeitschrift, Jahrgang 30. Heft 2.

Swallow, J. C. 1969. A deep eddy off Cape St. Vincent. Deep-Sea Research 16 (Supl.): 285–295.

Tomczak, M., and Godfrey, J. S. 1994. Regional Oceanography: An Introduction. Pergamon, New York. 422 pp.

Traganza, E. D., Nestor, D., and McDonald, A. 1980. Satellite observations of a nutrient upwelling off the coast of California. Journal of Geophysical Research, 85: 4104–4106.

Trenberth, K. E., Large, W. G., and Olson, J. G. 1990. The mean annual cycle in global ocean wind stress. Journal of Physical Oceanography, 20: 1742–1760.

UNESCO 1991. Processing of Oceanographic Station Data. UNESCO memorgraph by JPOTS editorial panel.